Instability of certain shear flows in nematic liquids*

Pawel Pieranski and Etienne Guyon
Laboratoire de Physique des Solides, Université Paris-Sud, 91405 Orsay, France
(Received 2 August 1973)

We have studied the simple shear flow, in the laminar regime, of a nematic (uniaxial) liquid film between two glass plates with carefully imposed boundary conditions. In the case considered here, the optical axis at rest is normal both to the flow velocity and to the velocity gradient. Using various methods of optical observation, we find the following facts: (a) When the shear rate s is below a certain threshold s_c, the optical axis is unperturbed everywhere. When $s > s_c$, it becomes distorted. s_c is inversely proportional to the sample thickness. (b) When a stabilizing field H is applied, s_c increases. Furthermore, above a certain limiting field H_L, the nature of the instability changes: a pattern of *rolls* appears, the rolls being parallel to the (average) flow lines. These effects are then explained in terms of the Ericksen-Leslie-Parodi equations describing the couplings between orientation and flow in a nematic fluid. This analysis has led in turn to the prediction and observation of other remarkable effects occurring when the shear rate is modulated (at low frequencies) and when *two* fields H (magnetic) and E (electric) are applied at right angles.

I. INTRODUCTION

A nematic liquid crystal is an anisotropic liquid made of long rodlike molecules which are aligned along one direction, without ordering of their centers of gravity. This alignment is associated with a strong birefringence: the local direction of alignment (usually labeled by a unit vector $\vec{n}$, called the director) is easily observable optically.[1]

Being a liquid, a nematic can flow (the viscosities being typically in the range of 0.1 P). There are two complications for these flows: (a) the friction coefficients are anisotropic; (b) there is a coupling between the orientation [described by the director $\vec{n}(\vec{r})$] and the flow [described by the velocity field $\vec{v}(\vec{r})$]. This coupling is described qualitatively for three typical situations, to be discussed in detail further in Fig. 1.

From a more formal point of view, the hydrodynamics of the coupled fields $\vec{v}(\vec{r})$ and $\vec{n}(\vec{r})$ have been written in detail by Ericksen,[2] Leslie,[3] and simplified by Parodi[4,5] (ELP). The constitutive equations involve five friction coefficients and are summarized in Appendix A.

These coefficients can be measured, in principle, from the study of various laminar flows. However, it is very important to work with channels where (i) the alignment of the director $\vec{n}$ is well defined—this can be done either through the influence of strong external fields or from the definition of boundary conditions (by suitable surface treatments); (ii) the geometry is simple enough (for instance channels of circular cross section lead to complicated director fields[6] and are not convenient); (iii) the channel thickness is small (typically 500 μ)—the sample is then quite transparent and the alignment can be monitored by various optical techniques. Most of the early experiments on flow in nematics did not satisfy these requirements; in general, the flow takes place in the presence of a large number of defects.

The first important progress was achieved by Miesowicz[7] in 1946 who used a strong field H to impose the molecular alignment in shear-flow experiments in nematic para asoxy anisole (PAA). For the three geometries of Fig. 1 he obtained values for the viscosities η_A, η_B, η_C. Recently, Gähwiller[8] has extended these measurements to methoxy p-n benzilidene butyl anilin (MBBA), which has a nematic phase around room temperature and which will be referred to in the rest of this paper. He found

$$\eta_a = 41.6\times 10^{-2}\ \text{P}\ ,$$

$$\eta_b = 23.8\times 10^{-2}\ \text{P}\ ,$$

$$\eta_c = 103.5\times 10^{-2}\ \text{P}\ .$$

Shear-flow studies in the absence of any aligning field H are more difficult since they require excellent surface conditions. These studies have been initiated by a theoretical calculation of Leslie.[9] The case of Fig. 1(c) has been studied optically by Wähl and Fischer.[10] In this case, as soon as a shear (the shear rate is $s = dv/dz$) is applied, the director field is distorted progressively. For low shears, the torque is given by $\alpha_2 s$. A similar result applies in the case of Fig. 1(b) but the corresponding torque $-\alpha_3 s$ is usually much smaller. In very large shear, the molecules tend to align at a small angle with the horizontal axis. This angle is given by $\tan^2\theta_0 = \alpha_3/\alpha_2$. For MBBA, Wähl

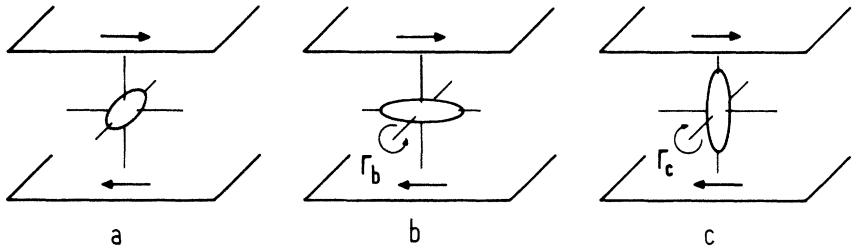

FIG. 1. Three shear-flow geometries. In case *b* and *c*, a torque is exerted on the director due to the shear. In the case *a* studied here, no torque exists below a critical threshold.

and Fischer find $\theta_0 \sim 8.2°$. Another determination by Meiboom and Hewitt[11] gives $\theta_0 = 15°$. (From the results of Gähwiller, one gets $\theta_0 \sim 7°$.)

The case of Fig. 1(a) is discussed in the present paper. The detailed experimental methods adequate to this geometry are presented in Sec. II. One finds that at low shear rates the director field is *not* altered; in this regime, there is no difference in hydrodynamic behavior between the nematic and an isotropic fluid of viscosity η_A. At higher shear rates, however, we have found that an instability takes place progressively above a threshold s_c; the director field becomes distorted.[12]

It may be helpful, at this stage, to present a relatively simple picture of the instability based on the hydrodynamic torques on Figs. 1(b) and 1(c). We start with the unperturbed director $\vec{n}_0$ normal to the flow lines and to the velocity gradient (Fig. 2). Let us then assume that a small fluctuation has rotated $\vec{n}$ from $\vec{n}_0$ to $\vec{n}_1 = \vec{n}_0 + \vec{n}_z (|\vec{n}_z| << |\vec{n}_0|)$ in a plane normal to the flow line (xz); the flow will create a torque Γ_z which tends to displace the extremity of $\vec{n}_1$ along the flow lines and will thus bring $\vec{n}_1$ to $\vec{n}_2 = \vec{n}_1 + \vec{n}_y (|\vec{n}_y| << |\vec{n}_0|)$. At this stage let us look at the projection of $\vec{n}$ on the yz plane: clearly we are in the situation described by Fig. 1(b) and according to the sign of the torque Γ_y shown on it, $\vec{n}_2$ moves towards $\vec{n}_3 = \vec{n}_2 + \vec{n}_z'$, thus increasing n_z. So if we started with a small deviation $\vec{n}_1 - \vec{n}_0 = \vec{n}_z$ parallel to z we obtain at the end an increase of this deviation measured by $\vec{n}_3 - \vec{n}_2$; this shall lead to an instability.

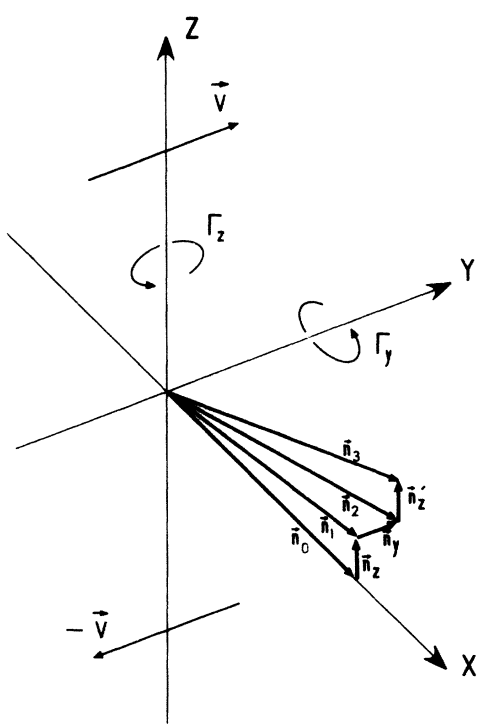

FIG. 2. Mechanism for the development of an instability in the case of Fig. 1(a). An initial fluctuation n_z is further amplified to $n_z + n_z'$ via an n_y distortion.

The argument above holds for an infinite sample. For a film of finite thickness with $\vec{n}$ anchored at both limiting plates, the distortion is not uniform along z and requires some Frank elastic energy.[13] The instability will occur only when the destabilizing hydrodynamic torques exceed the restoring elastic ones. There will be a threshold rate s_c below which the system stays unperturbed. The problem is analogous to the distortion transition of an aligned nematic under the influence of a perpendicular magnetic field (Fredericks transition[14]).

The instability we have just described leads to a director field $\vec{n}(z)$ (invariant under translations in the xy plane of the slab). We shall call this an "homogeneous distortion." The associated flow lines remain parallel to the unperturbed flow direction y. This homogenous distortion effect has been reported briefly in a preceding paper[12] and will be described in more detail in Sec. III. We have also investigated the instabilities occurring under applied external fields and with shear rates s which are modulated in time; we have found that a second type of instability can occur. It involves rolls of circulation having their axis parallel to the flow. This roll instability is presented in Sec. IV. A simplified theoretical interpretation is proposed in Sec. V. In the conclusion, we present a comparative discussion with the case of electrohydrodynamic convection in nematics. In the appendixes we summarize the continuum viscoelastic theory used and we apply it to our shear-flow problem.

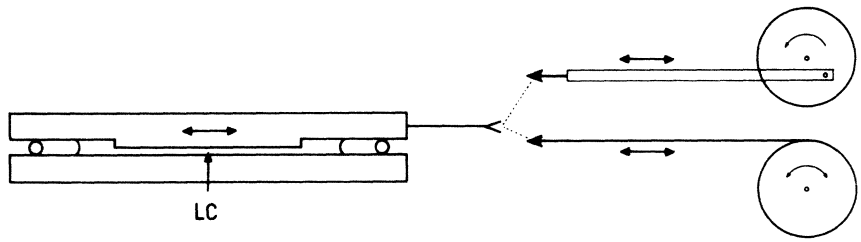

FIG. 3. Schematic of the shear-flow experimental setup.

II. EXPERIMENTAL

A representation of the flow cell is given in Fig. 3. The two horizontal transparent cells ($5\times2\times1$ cm) can slide relative to each other. The maximum available displacement is of the order of 2 cm. In the ac experiments, one plate moves with respect to the other with a sinewave motion; velocity $v=\frac{1}{2}(D/T)\cos(2\pi t/T)$. The variable rate is obtained by supplying a variable frequency voltage to a synchronous motor. A solid bar connects the moving plate to the motor where it is attached eccentrically to a pin at a distance from the axis of the motor (as in a steam engine). The variable amplitude of displacement is obtained by changing this distance. In the dc experiments, an unstretching string attached at one end to the movable plate is wound on a pulley connected to the motor. By using an inversion relay, it is also possible to use this system to get a square-wave motion.

The distance between the two plates is kept constant by using calibrated ball bearings as spacers. In order to get rid of back-flow effects in the active part of the cell, the liquid crystal (LC) completely fills the cell and also a thicker rim which exists all around it. The distortions which we will describe occur very uniformly over the cell, indicating that no appreciable edge effects take place.

The cell is placed between the polar plates of a magnet which provides a field up to 6 kG in the X direction.

The inner sides of the plates are precoated with thin transparent conducting Au films which can be connected to a voltage supply through thin conducting wires soldered to the Au, thus providing a vertical electric field across the cell. The vacuum evaporation of Au is carried under a 60° oblique incidence. This technique gives rise to a surface alignment of the molecules in the plane of the film ("planar") in a direction (X) perpendicular to the plane of incidence of the Au beam.[15,16]

The structure can be observed optically in the $0z$ direction with a microscope or by studying the diffraction on pattern of a laser beam. Conoscopic techniques[17] also provide an accurate description of the structures in uniformly aligned samples. Good samples, that had been submitted to shear flows for 100 h, would still give a perfect uniform alignment (no disinclinations) of uniaxial planar samples when the shear flow was stopped. This technical point is essential for the quality of the experiments described here.

III. HOMOGENEOUS INSTABILITY

A. Experiments

We consider the effect of a constant shear rate $s=dv/dz$ long after the shear has been applied. For $s<s_c$, the conoscopic image formed of two

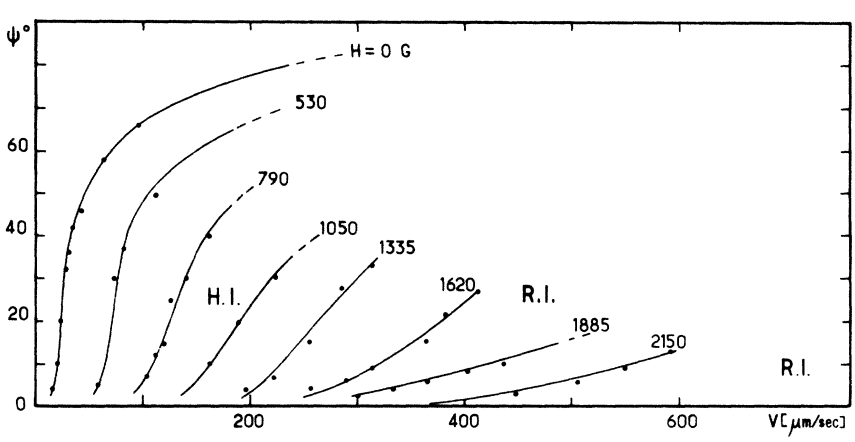

FIG. 4. Rotation of the planar conoscopic image, measured by ψ (proportional to n_y) as a function of a constant shear velocity v for a 200-μ-thick layer. The curve $H=0$ corresponds to that given in Ref. 12. When the (stabilizing) field H increases, the threshold increases. Also the range of existence of the homogeneous instability (H.I.) decreases. The right-hand part of the diagram corresponds to the domain of existence of a roll instability (R.I.).

sets of hyperbolas characteristic of a uniaxial planar sample is unchanged by the flow (this implies in particular that no defects are introduced by the flow). When $s > s_c$, the conoscopic image rotates by an angle ψ. This rotation can be associated to a twist of the average director in the xy plane, characterized by a polar azimuthal angle Φ. Together with the rotation, the center of the hyperbolas is displaced along y. This is associated to a vertical component of $\vec{n}$ (polar angle θ).

Figure 4 gives the variation of ψ vs s for different values of the field H applied along $0x$. We consider first the curve $H=0$ which is similar to that given, with a larger scale, in Ref. 12. Below a critical value s_c, ψ (and Φ) remains zero. Neglecting the tail at low ψ due to small misalignments, the linear variation above s_c is characteristic of a second-order phase transition. For large s, the limiting value of ψ corresponds to an angle $\Phi = \frac{1}{2}\pi$; except for two boundary layers where the orientation twists back to the value $\Phi = 0$ imposed by the walls, the molecules are in the vertical plane of the velocities. In this plane, the molecules are at an angle $\sim\theta_0$ with y, and we indeed recover the Leslie conditions (except for the two thin boundary layers). A measurement of the lateral motion gives a rather inaccurate picture of the transition because the angle θ_0 is small. However, for large shear rate, our θ_0 estimates agree with the data already reported.

The other curves are given for increasing magnetic fields. The increase of threshold is consistent with the fact that the field is stabilizing (it tries to keep the molecules along x). High enough above the threshold, the homogeneous mode is replaced by a periodic roll structure. If the field is large enough, the homogeneous distortion never takes place and the roll structure occurs just above the threshold. The roll instability will be discussed in Sec. IV.

Remark. In order to build up a homogeneous state, we let a small angle between the unperturbed $\vec{n}_0$ and the normal to the flow. If $\vec{n}_0$ is exactly perpendicular to the flow, two equivalent distortions symmetric with respect to the yz plane can take place involving the formation of walls along y. However, these domains are not distributed uniformly in space and cannot be mistaken with the regular roll structures.

B. Interpretation

The instability threshold is obtained by balancing the hydrodynamic torques against the elastic and magnetic torques. If we assume a permanent regime, a homogeneous sample, and no velocity components along x and z, the hydrodynamic torque expressed in Eq. (A15) reduces to $\Gamma_{\text{hydro}} = (0, -\alpha_3 s n_y, \alpha_2 s n_z)$. The two components of the torque express quantitatively the effect of the two acting components n_y and n_z along y and z described in Sec. I. Effects such as the variation of the shear rate with z would give higher-order contributions. Balancing this torque against the elastic and magnetic ones, gives the coupled equations

$$-\chi_a H^2 n_z + K_1 \frac{d^2 n_z}{dz^2} = \alpha_3 s n_y , \tag{3.1}$$

$$-\chi_a H^2 n_y + K_2 \frac{d^2 n_y}{dz^2} = \alpha_2 s n_z , \tag{3.2}$$

where K_1 and K_2 are the Frank constants for the splay distortion due to the variation of n_z and for the twist due to that of n_y.

We look for solutions that satisfy the boundary conditions $n_y = n_z = 0$ for $z = \pm\frac{1}{2}d$. The lowest threshold is obtained for the most slowly varying solution

$$n_z/n_{z_0} = n_y/n_{y_0} = \cos \pi z/d .$$

Using these forms of n_z and n_y, we obtain the threshold from the compatibility condition of Eqs. (3.1) and (3.2),

$$\alpha_3 \alpha_2 s_c^2 = (K_1 \pi^2/d^2 + \chi_a H^2)(K_2 \pi^2/d^2 + \chi_a H^2) , \tag{3.3}$$

which reduces in zero field to

$$s_c d = v_c d^2 = \pi^2 (K_1 K_2/\alpha_2 \alpha_3)^{1/2} . \tag{3.4}$$

In high fields, where the elastic torques are small compared to the magnetic ones, expression (3.3) simplifies to

$$s_c/H^2 = \chi_a/\alpha_2 \alpha_3 . \tag{3.5}$$

The experimental results have already been described in Ref. 12. For a $d = 200$-μ-thick film, we obtain, *in zero field,* a critical velocity $v_c = 11.5$ μm/sec. Using values of $K_1 = 6.1 \times 10^{-7}$ cgs, $K_2 = 2.9 \times 10^{-7}$ cgs, we obtain $(\alpha_2 \alpha_3)^{1/2} = 0.18$ cgs at 23°C. [Values of elastic constants of MBBA are given in table form in the book by de Gennes (Ref. 1).] The *high-field* results are well described by law (3.5) with $s_c/H^2 = 6.6 \times 10^{-7}$ cgs. Using $\chi_a = 1.12 \times 10^{-7}$ at 23 °C, we find a second determination $(\alpha_2 \alpha_3)^{1/2} = 0.17$ cgs, which agrees reasonably well with our first value and with other published results.[8,10,11]

IV. ROLL INSTABILITIES

A. Modes of production

If a large enough stabilizing magnetic field is applied on a dc shear flow, the homogeneous distortion is never obtained. Above a certain threshold, the instability appears as a very regular series

of lines *parellel to the velocity* and strongly reminiscent of the Williams convection rolls observed in an electric field,[18,19] or of the thermal convective instability, observed in planar samples.[20] The spacing of the lines is of the order of magnitude of the thickness of the cell and does not vary much when external conditions are changed. The lines are alternatively bright and dark due to the difference in the diffracted light by the lenses formed by the up and down parts of the structure distorted along x.

Another way of obtaining this structure is to apply an ac shear. In this case, the instability is obtained even in zero magnetic field. (Obviously, the homogeneous mode must be found again if the shear rate is low enough so that it comes close to a dc experiment.)

For the sake of completeness, we should also mention the formation of rolls when a dc shear much larger than the threshold is applied. However, in the present paper, we want to restrict our description to threshold problems and we will analyze in detail only the two first regimes.

B. Properties

Like the other convective instabilities on planar LC samples, the rolls cannot be observed in light polarized perpendicular to the molecules. The regular structure can be followed from the diffraction pattern of a parallel laser beam sent perpendicular to the film. A set of diffraction points regularly spaced and aligned perpendicular to the rolls axis can be seen on a screen. We have observed diffraction spots up to the 30th order. (A similar diffraction pattern can be obtained by applying on the same sample an electric field of suitable frequency and amplitude in the Williams regime but we have not found as extended diffraction patterns in the latter case.) It is possible that the mechanical displacement of the plate favors the organization of the domain. The existence of diffraction spots of high order means that the distortion in nonsinusoidal.[21] Indeed, when we are close from the threshold only a small number of diffraction orders is obtained. The appearance of this diffraction pattern gives the most sensitive test of appearance of convection especially if a photocell is used to measure the scattered intensity.

A careful observation of the rolls obtained in ac flow shows that two types of roll instabilities can be found.

(i) In the first regime, the bright and dark lines do not alternate from one half-period to the next. This proves that the quantity n_z, which characterizes the vertical distortion, does not change sign.

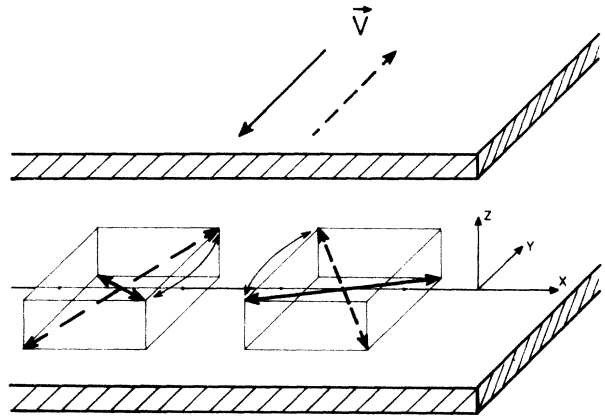

FIG. 5. Y regime in an ac shear flow.

The formation of double images of dust points localized below the lower face of the LC can also be used to study the distortion of the director. In this regime, the direction of the alternate displacement of the extraordinary image can be used to show that the horizontal component n_y changes sign at each period. We will call this *regime Y*.

(ii) In a second regime, we see an alternation of bright and dark lines at each half period. In this regime, n_z changes sign but not n_y. We call it the *regime Z*.

It is also possible to characterize the two regimes from a study of the time dependence of the intensity of one diffraction spot.

The Figures 5 and 6 give a schematic representation of the two regimes. The conditions selecting one regime against the other will be analyzed after the theoretical discussion in Sec. V.

V. INTERPRETATION AND SYSTEMATIC EXPERIMENTS

A. Existence of a roll instability

Compared to the homogeneous distortion, the roll instability involves an increase of the elastic energy due to the bend of the molecules along $0x$. However, we know that, in large enough fields, the elasticity plays a minor role. Rolls should form more easily in this case if we are able to find new destabilizing mechanisms associated with the distortion along $0x$. Several such terms can be found in the force equations obtained in the Appendix B. We will restrict here our discussion to the case of the roll instabilities obtained in dc experiments in high magnetic field ($\dot{n}_y = \dot{n}_z = 0$) and we consider only the new terms involved in evaluating the distortion along x. We find the following forms:

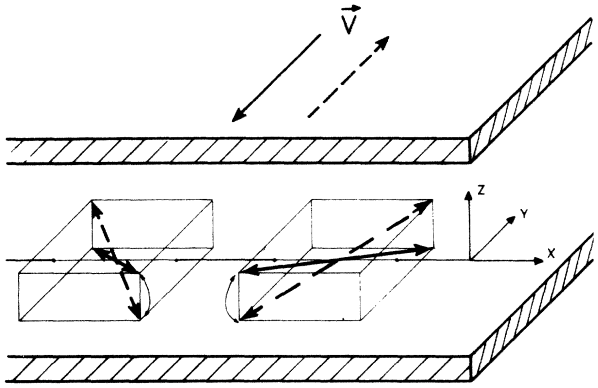

FIG. 6. Z regime in an ac shear flow.

$$F_y = \eta_c \frac{\partial^2 v_y}{\partial x^2} + \frac{\alpha_5 - \alpha_2}{2} s \frac{\partial n_z}{\partial x} , \tag{5.1}$$

$$F_z = \eta_c \frac{\partial^2 v_z}{\partial x^2} + \frac{\alpha_5 + \alpha_2}{2} s \frac{\partial n_y}{\partial x} . \tag{5.2}$$

The first terms are classical frictions giving the effect of the velocity perpendicular to the molecules. The second terms describe a new coupling mechanism. Due to the distortion of n_y along $0x$, the shear will induce a velocity field v_z (a certain kind of hydrodynamic focusing effect) given by

$$\eta_c i k_x \frac{\partial v_z}{\partial x} + \frac{\alpha_5 + \alpha_2}{2} s\, i k_x n_y = 0 .$$

$k_x(k_z)$ is the magnitude of the wave vector of the distortion along $x(z)$. The velocity $v_z(x)$ will create a new *destabilizing* hydrodynamic torque acting on the component n_z:

$$\Gamma_y = -\alpha_2 \frac{\partial v_z(x)}{\partial x} = \frac{\alpha_2(\alpha_2 + \alpha_5)}{2\eta_c} s n_y .$$

We can write finally the torque equations along y and z as

$$-(\chi_a H^2 + K_1 k_z^2 + K_3 k_x^2) n_z = \alpha_3 s n_y - (\alpha_2/\eta_c)\tfrac{1}{2}(\alpha_2 + \alpha_5) s n_y , \tag{5.3}$$

$$-(\chi_a H^2 + K_2 k_z^2 + K_3 k_x^2) n_y = \alpha_2 s n_z - (\alpha_2/\eta_c)\tfrac{1}{2}(\alpha_5 - \alpha_2) s n_z . \tag{5.4}$$

This differs from the homogneous case [forms (3.1) and (3.2)] by the addition of the elastic terms on the left-hand side and of hydrodynamic terms specific of the roll structure. We will have a homogeneous, or a roll instability, depending on what contribution is largest. If we assume a one-constant approximation ($K_1 = K_2 = K_3$), the threshold condition for rolls reduces to

$$s^2_{\text{roll}} = \frac{(\chi_a H^2 + K k_x^2 + K k_z^2)^2}{\alpha_2 \alpha_3 (1+g)} = s^2_{\text{hom}} \frac{[1 + K k_x^2/(\chi_a H^2 + K k_z^2)]}{1+g} , \tag{5.5}$$

with

$$1 + g = \left(1 - \frac{\alpha_2(\alpha_2 + \alpha_5)}{2\alpha_3 \eta_c}\right)\left(1 - \frac{\alpha_5 - \alpha_2}{2\eta_c}\right) ,$$

$g \sim 3$ to 3.5.

This should be compared to the threshold $s^2_{\text{hom}} = (\chi_a H^2 + K k_z^2)/\alpha_2 \alpha_3$ for the homogeneous instability. In large fields, *the roll distortion will always be more favorable* because of the reduction by the factor $(1+g) > 1$ in s^2. In zero field, the solution will depend on the ratio

$$x = (k_z^2 + k_x^2)/k_z^2(1+g)$$

as compared to unity. The experiments indicate that $x > 1$ so that the homogeneous solution is preferred for $H = 0$. Let us assume $k_x = k_z$. This implies that g should be smaller than one. In fact, if we use an estimate of the field $H_L \sim 3$ kG for the sample of Fig. 4, the formula (5.5) would imply a value g of the order of 0.1. It is not possible at the present stage to resolve the discrepancy as the result depends critically on the ratio k_x/k_z as well as of the back flow which should limit the destabilizing effect of v_z. These two contributions have not been considered in the qualitative analysis of this paper.

B. Phenomenological equation for n_y and n_z

An analysis of the hydrodynamic equations for the shear-flow problem based on the Ericksen-Leslie-Parodi (ELP) equations (introduced in Appendix A) is given in Appendix B. We can include the effect of the velocity field—the back flow effects[22]—by renormalizing the viscosity. A quantitative theoretical approach could be carried along lines parallel to the problem of electrohydrodynamic instabilities where both one-dimensional (only variations along x are considered)[23,24] and two-dimensional (along x and z)[25] numerical solutions have been obtained. An exact solution involves a proper self-consistent consideration on the boundary conditions for $\vec{n}$ and $\vec{v}$ at the limiting plates and leads in particular to the determination of the wave numbers of the distortion along x and z at the threshold. The quantitative fit of a calculation with experimental thresholds gives access to estimates of various combinations of viscosity coefficients. We are concerned here with the description of the physical mechanism of the distortion and will use a phenomenological treatment which will give us access to the electric and

magnetic field dependence of the threshold as well as to the amplitude and frequency dependence in the ac regime. However, we will not try to get any determination of viscosities (except for order-of-magnitude checks).

Equations (B6) and (B7) can be written in the following concise form:

$$\dot{n}_y + n_y/T_y + A\, s n_z = 0\ , \tag{5.6}$$

$$\dot{n}_z + n_z/T_z + B\, s n_y = 0\ , \tag{5.7}$$

where

$$\frac{1}{T_y} = \frac{1}{T_{y_0}} + \frac{\chi_a H_x^2}{\gamma_y}\ , \tag{5.8}$$

$$\frac{1}{T_z} = \frac{1}{T_{z_0}} + \frac{\chi_a H_x^2}{\gamma_z} - \frac{\epsilon_a E_z^2}{\gamma_z}\ . \tag{5.9}$$

T_{y_0} and T_{z_0} take into account only the effect of the elastic contribution $T_0 \sim \gamma/Kk^2$, whereas the following terms express the reduction of the time constant when the *stabilizing* fields H_z and E_z are applied. The effect of the elastic time constant is of the order of magnitude of the magnetic (or electric) one for fields values corresponding to the Fredericks threshold $H_c = (\pi/d)(K/\chi_a)^{1/2}$.[14] This corresponds to values $V_c \simeq 3$ V, $H_c = 400$ G for a 300-μ-thick film. For $H \gg H_c$ or $V \gg V_c$ the elastic contribution can be neglected.

Under this form, our ac shear flow instability problem is formally similar to that of the electric instability in an ac electric field. In the latter case, we also have two coupled variables; the density of charges q and the local curvature ψ of the director field. The equations for q and ψ are equivalent in form to Eqs. (5.6) and (5.7), the meaning of the relaxation times being of course different. We have used an analysis developed for the (q, ψ) system by Galerne[26] for the simple square-wave-case excitation. We consider the set of equations equivalent to Eqs. (5.6) and (5.7),

$$\dot{n}_y + n_y/T_y + A\, s n_z = 0\ , \tag{5.10}$$

$$\ddot{n}_y + \dot{n}_y\left(\frac{1}{T_y} + \frac{1}{T_z}\right) + n_y\left(\frac{1}{T_y T_z} - A\, B s^2\right) = 0\ . \tag{5.11}$$

Galerne looks for solutions of n_y of the form

$$n_y = N_1 e^{-t/t_1} + N_2 e^{t/t_2} \tag{5.12}$$

and

$$A\, s n_z = N_1\left(\frac{1}{t_1} - \frac{1}{T_y}\right) e^{-t/t_1} - N_2\left(\frac{1}{t_2} + \frac{1}{T_y}\right) e^{t/t_2}\ . \tag{5.13}$$

We assume a square wave variation of v with a period T,

$$v = +v_0 \quad \text{for } 0 < t < \tfrac{1}{2}T\ ,$$

$$v = -v_0 \quad \text{for } \tfrac{1}{2}T < t < T\ ,$$

Two types of solutions can be obtained. (a) In the regime Y, only the component n_y changes sign through a period. At the end of half a period we write the conditions

$$n_y(\tfrac{1}{2}T) = -n_y(0), \quad n_z(\tfrac{1}{2}T) = n_z(0)\ ,$$

which leads to

$$\left(\frac{1}{t_2} + \frac{1}{T_y}\right) \coth\frac{T}{2t_2} = \left(\frac{1}{t_1} - \frac{1}{T_y}\right) \coth\frac{T}{2t_1}\ . \tag{5.14}$$

(b) The other regime Z is such that $n_y(\frac{1}{2}T) = n_y(0)$ and $n_z(\frac{1}{2}T) = -n_z(0)$. Then

$$\left(\frac{1}{t_2} + \frac{1}{T_y}\right) \tanh\frac{T}{2t_2} = \left(\frac{1}{t_1} - \frac{1}{T_y}\right) \tanh\frac{T}{2t_1}\ . \tag{5.15}$$

It is easily shown and understood that if the relaxation-time constant T_y is smaller than T_z, we can find solutions of (5.10) and (5.11) satisfying (5.14) but not (5.15). That is to say, n_y will oscillate around zero and not n_z. This is our regime Y. If $T_y > T_z$, the solutions satisfy the other periodicity condition (5.15). Only n_z oscillates around zero (corresponds to regime Z). The intermediate regime where both n_y and n_z oscillate around zero can only be found when $T_y/T_z = 1$. We will postpone the discussion of the results of these equations after the presentation of the experiments.

C. Alternating case: experiments

In our experiments, the displacement of the upper plate is sinusoidal and may be written $\frac{1}{2}D \times \cos 2\pi t/T$, where D is the total displacement. In order to make an approximate comparison between our results and the simplified square wave model discussed in the previous paragraph, we chose to put the shear velocity $v = sd$ in the square wave model equal to $2D/T$. For a fixed D/T, the threshold is studied as a function of the frequency T^{-1}.

The effect of a magnetic field along the x axis and of an electric field along (oz) has been studied systematically. We have produced E_z using a 10-KHz ac voltage supply up to 100 V. At this high frequency and low voltage, the electric field by itself does not give rise to instabilities but only tends to align the molecules perpendicular to it (as $\epsilon_a = \epsilon_\parallel - \epsilon_\perp < 0$). Figure 7 gives a series of experimental threshold curves for different values of D/T as a function of E and T^{-1}. The magnetic field was kept constant ($H = 3200$ G). This figure constitutes the central result of this paper.

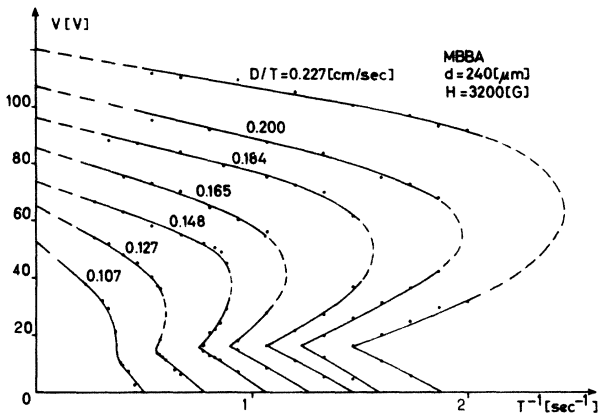

FIG. 7. Experimental roll instability threshold curves for different values of the effective velocity D/T as a function of the frequency T^{-1} of the sine wave shear and of the transverse applied voltage.

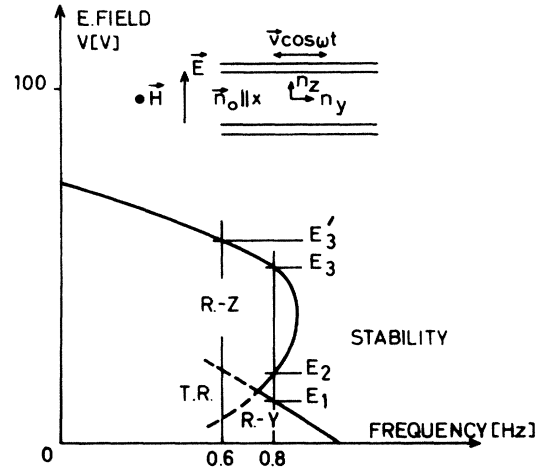

FIG. 8. Curve $D/T = 0.148$ of Fig. 7 has been reproduced in order to show the different instability regimes (R-Y = Y regime; R-Z = Z regime).

We restrict our attention to a curve for a given value of $D/T = 0.148$ cm/sec, which is reproduced in Fig. 8. For a given electric field, the instability is present only if the frequency is lower than a certain value (to the left of the curve). For large frequencies, there are no instabilities (the instabilities have not time to develop in half a period). The most spectacular feature of the curve is the existence of two branches. We keep the frequency constant, $1/T = 0.8$, and increase E. In the absence of electric field, the instability is present. It is of the Y *type*. At a certain value of field E_1 the instability disappears. For an even larger value E_2, the instability reappears but it is now of the Z *type*. Finally, for the value E_3, the Z instability disappears. The spatial period of the rolls remains always of the order of the film thickness in the three branches but it is usually larger (by 20%) in the branch 2. We have not done any systematic study of this effect, in the absence of a specific model.

At a frequency slightly smaller than that of the cusp ($1/T = 0.6$), the instability is still of the Y type for $E = 0$. In larger fields, it is Z type. It disappears at a critical field E_3'. This branch is the continuation of the E_3 branch. The switching between Y and Z regime takes place in a domain which is defined from the extrapolation of the thresholds branches 1 and 2 to the left. This intermediate domain (T-R *in* Fig. 8) is characterized by some "exotic" structures; the rolls do not extend over long distances but cross in a rather regular way. This corresponds to the interchange between the Y and Z type instability along a given roll. The diffraction pattern instead of showing a single set of points along the axis ox, now contains *satellite* spots in the direction *oy*. In addition, the diffraction pattern shows peaks twice as closely spaced as in the regular case indicating the existence of a doubled spatial period along *ox* which we intend to described more intensively later.

The threshold curve can be qualitatively easily understood in terms of a comparison of T_y and T_z. For $E = 0$, we have the Y instability and $T_y/T_z < 1$. As E increases, T_y/T_z also increases.

The cusp, where the instability does not develop easily,[27] is observed when the two times T_y and T_z become equal. In larger fields such that $T_y/T_z > 1$, the Z instability develops. However, if the electric field becomes large, T_z is quite small and the Z instability relaxes rapidly to zero. We can see that by considering the zero-frequency extrapolation of branch 3. In this dc regime, the result (3.3) should apply indicating that the threshold varies as $(T_y T_z)^{-1/2}$. Increasing the electric field increases this threshold and unfavors the instability.

If we come back to the set of curves of Fig. 7, we see that large effective velocities D/T imply indeed that the instabilities are obtained up to larger frequencies.

The value of the electric field at the cusp E_B is the same for different D/T. This is an important test of the validity of our description; the condition $T_y/T_z = 1$ leads to a well-defined value of E_B, independent of the velocity D/T, once H is specified.

D. Comparison with square wave model

In order to compare the experiments with the model, we have to define the values of the following parameters:

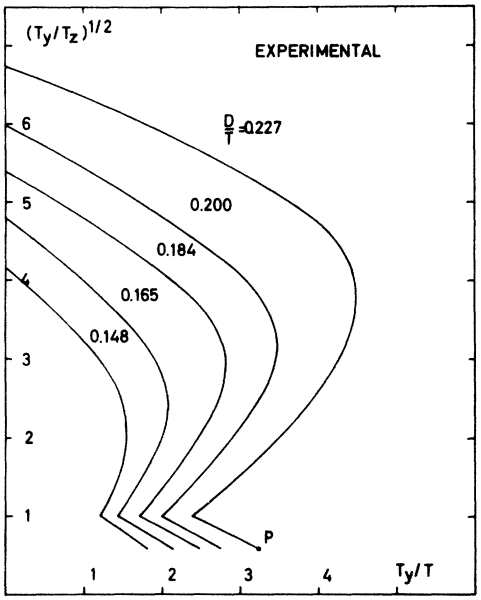

FIG. 9. Experimental results of Fig. 7 plotted in reduced units.

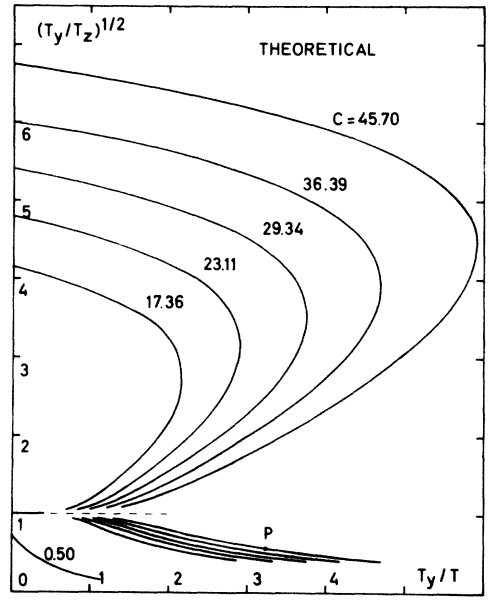

FIG. 10. Results of the calculation of the square wave model with parameters fitted to the results of Fig. 8 by adjusting the zero frequency value, the cusp one, and one point P to define the frequency scale.

$$\frac{T_y}{T_z}, \quad \frac{T_y}{T}, \quad A B s^2 T_y^{\,2} = C \ .$$

The first parameter defines the type of regime obtained. The second expresses the frequency of the ac shear in reduced units. The last one gives the critical shear rate s in units comparable to those used in the discussion of the homogeneous threshold $s_{\text{hom}} = (AB/T_y T_z)^{1/2}$ [Eq. (5.16)]. We neglect the changes of T_y due to the variation of the wave vector of the distortion along x. The sets of curves of Fig. 7 have to be expressed in units T_y/T_z vs T_y/T and compared with a calculated curve with the appropriate value of C. This can be done by fitting two points. We take one curve.

At the cusp point, we have

$$\frac{T_y}{T_z} = \frac{\gamma_y/\chi_a H^2}{\gamma_z/(\chi_a H^2 + \epsilon_a E_B^{\,2})} = \frac{\gamma_y}{\gamma_z}\,\frac{\chi_a H^2 - \epsilon_a E_B^{\,2}}{\chi_a H^2} = 1 \ .$$

And at the point of intercept with $T^{-1} = 0$ (obtained by extrapolation of branch 3)

$$\frac{T_y}{T_z} = \frac{\chi_a H^2 - \epsilon_a E^2}{\chi_a H^2 - \epsilon_a E_B^{\,2}} = A B s^2 T_y^2 = C \ . \qquad (5.16)$$

(We have neglected the elastic contribution which is negligible for the data of Fig. 7.)

Finally, we normalize the axis of frequencies using a particular point (P) of Fig. 9 to the calculated curve. (The same normalization is then used for all curves.)

Figures 9 and 10 give the experimental and calculated curves in these reduced units. We see a general qualitative agreement between the two sets of curves. However, the calculated curve for the square model displays a more pronounced cusp structure than the experimental ones for a sine wave excitation. A similar difference had been found in the case of electrical instabilities, to be reviewed later (see Fig. 15), where the experimental and calculated threshold curves indicate more pronounced structures for a square wave excitation. However, we have also done some preliminary experiments using square wave shear. The results are close to the corresponding sine wave experiments. It is not possible to conclude, at the present time, on the nature of the quantitative discrepancies with the simplified model.

The existence of the cusp appears clearly in the model. In Fig. 11, we have used an enlarged vertical scale to display the result of the calculation. We see that no instability can develop when $T_y/T_z = 1$. This cusp, going to zero frequency, is very sharp and would be probably very hard to detect due to the heterogeneities of the fields.

E. Further results

We have complemented this discussion of the ac effects by a further analysis of some of the parameters of the problems.

1. *Magnetic field*

Figure 12 presents a series of threshold curves obtained for different values of the magnetic field

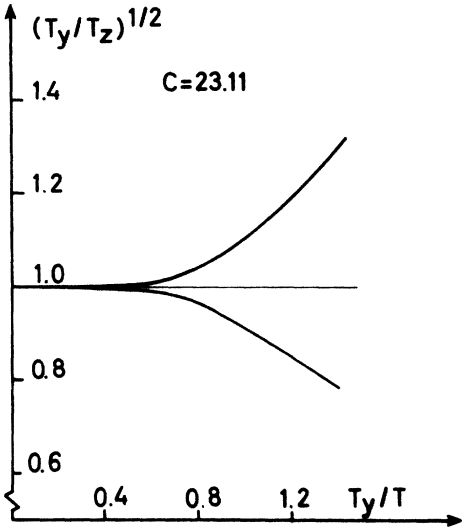

FIG. 11. Detailed representation of the calculated curve. The cusp going to zero frequency (no instability when $T_y/T_z=1$) is particularly sharp.

while keeping the amplitude D/T fixed. For a given electric field, the threshold frequency decreases for larger values of stabilizing magnetic field. We also see that the electric field at the cusp E_B increases with H (whereas E_B remains constant when D/T varies for a constant H).

The condition $T_y/T_z=1$ at E_B is written

$$\frac{1}{T_{y_0}}-\frac{1}{T_{z_0}}+\chi_a H^2\left(\frac{1}{\gamma_y}-\frac{1}{\gamma_z}\right)=-\frac{\epsilon_a E_z^{\,2}}{\gamma_z}\,. \quad (5.17)$$

Figure 13 shows the results obtained from Fig. 12 in units $V_B^2(H^2)$. They are consistent with the linear variation of Eq. (5.17) and show the two following features: the slope is positive and γ_y is smaller than γ_z; the elastic time constant T_{y_0} is shorter than T_{z_0}.

In the Leslie analysis developed in the appendixes, we obtain $\gamma_y \sim \gamma_z$. This was a reasonable result since the displacements along y and z give similar back-flow effects if we do not consider the boundary effects for the velocity along oz. In fact, in the relaxation of n_y, the full "back-flow" effects, which tend to reduce the viscosity, take place whereas the presence of solid boundary along oz limit the contribution of the horizontal back-flow currents, and $\gamma_z > \gamma_y$ (for a complete calculation of this effect, see Ref 28). This lower value of γ_y also probably explains why the Y mode is found in the absence of field; the elastic torques for the relaxation of n_y are smaller than those for n_z, as n_y involves in particular a "twist" relaxation (the twist elastic constant K_2 is typically three times smaller than the two other constants K_1 and K_3). In order to overcome this effect, the

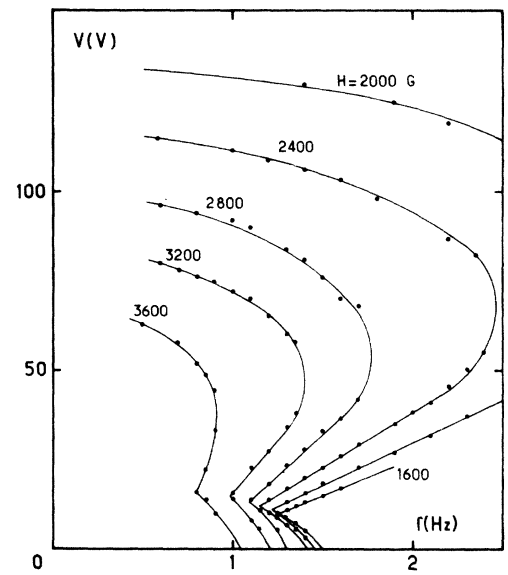

FIG. 12. Effective velocity has been kept constant ($2D/T=0.4$ cm/sec). When H increases, the domain of stability increases. Also the voltage at the cusp increases.

visocosity γ_y has to be sufficiently smaller than γ_z so that the time constant $T_{y_0}=\gamma_y/(K_2k_z^{\,2}+K_1k_x^{\,2})$ be smaller than T_{z_0}.

2. *Zero-frequency limit*

This limit can be obtained by extrapolating finite frequency data taken from curves such as that of Fig. 7. (When T^{-1} goes to zero, we must have large displacements D if we wish to keep D/T constant. This is our limitation in obtaining data at low frequency). We expect that the extrapolated values for $T^{-1}=0$ should not depend on the type of excitation and should also agree with the static re-

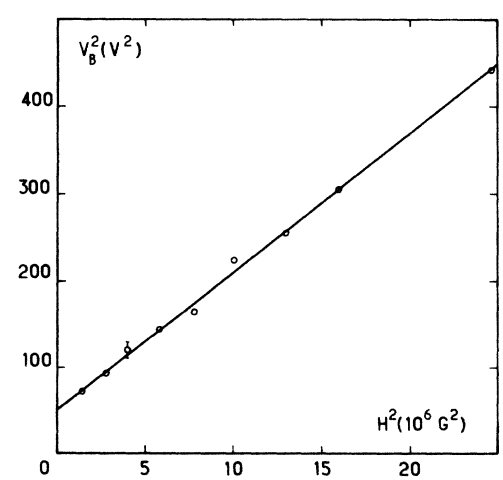

FIG. 13. Square of the cusp voltage V_B^2 varies linearly with H^2 as expected theoretically.

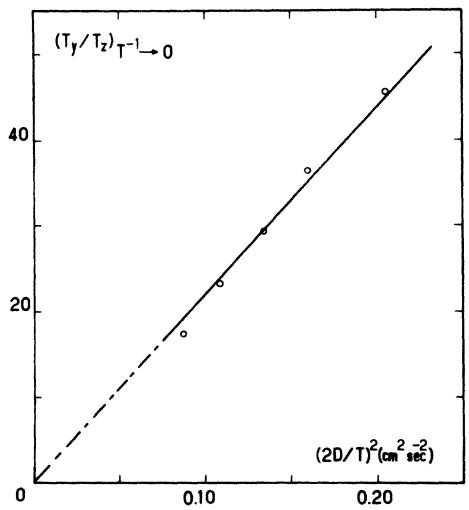

FIG. 14. In zero frequency the square of the effective velocity varies proportionally to T_y/T_z (deduced from the extrapolation of the experimental data of Fig. 9).

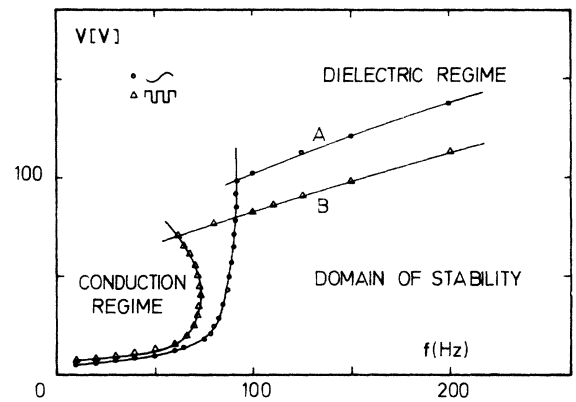

FIG. 15. Threshold voltage for the development of the electrodynamic instabilities as a function of frequency for both sine-wave and square-wave cases. The existence of a cusp separating the conduction and dielectric regimes is to be compared with the existence of the Y and Z regimes in our problem. The experimental data are from Galerne (Ref. 26) and the calculated curves from Dubois-Violette (Ref. 24).

sult $s=(AB/T_yT_z)^{1/2}$, where T_y and T_z are functions of the fields.

Equation (5.16) can be written

$$ABs^2T_y^2=T_y/T_z\,.$$

In Fig. 14, the experimental values of T_y/T_z taken from Fig. 9 in the limit $T^{-1}=0$ are found to vary linearly with the square of the effective velocity $(D/T)^2$. This result is consistent with the formula written above as T_y^2 is approximately constant for a given film thickness and magnetic field.

3. *Thickness dependence*

The results we have just discussed have been obtained with different samples having approximately the same thickness $d\sim 200\ \mu$. If we consider the model of Sec. III we see that the thickness comes indirectly into the model to define the values of the wave vectors k_x and k_z $(\sim 1/d)$ which play a role essentially in the elastic terms. In large electric and magnetic field, the elastic contribution becomes negligible. We then expect the results for different thicknesses to reproduce for the same value of the shear rate $s=v_{\max}/d$. The experimental results agree qualitatively with this prediction and the critical velocity characterized by D/T varies as d.

4. *Temperature*

Experiments were given for a temperature $T=(23\pm 1)^\circ$C. The threshold curves vary quite rapidly with T due to the rapid variation of the viscosity coefficients with T.

VI. CONCLUSION

The experiments reported here exhibit a new class of hydrodynamic instabilities of liquid crystals. We have limited our study to the problem of the development of linear instabilities controlled by external fields. Our experiments are qualitatively well described by the current hydrodynamic model of nematics. A quantitative analysis is clearly of interest and will give access to viscous constants but we feel that most of the essential features of the phenomenon described are obtained in this qualitative model. A study of the effect above threshold including in particular the problem of changes of regime $Y\to Z$ should also be developed. We should also mention the interesting aspect of the motion of disinclination lines in the structure. Some formal analogies can be drawn between these hydrodynamic instabilities and other convective effects under the influence of a thermal gradient[29,30] or of an electric field.[18,19,23–26] Such a discussion will be developed in a separate paper.[30] Let us just mention schematically the essential results obtained in the latter case. Here the convection is induced by the action of the electric field on charges q either injected via the electrodes or present in the liquid crystal.

A vertical curvature of the director, given by $\phi=\partial n_z/\partial x$, can be induced under the effect of the shear due to the convective flow and the local electrostatic field on the dielectrically anisotropic molecules. This curvature induces a local accumulation of charges because of the electrical conductivity anisotropy. In materials like MBBA this causes an increase of the local charge fluctua-

tion q. The coupled variables ϕ and q correspond to n_y and n_z in our problem. Two regimes are also met: in a first regime—*conducting*—the characteristic time for the relaxation of the director T_z is larger than T_{el}, the dielectric relaxation time. In an ac electric field, the charge oscillates around zero but the distortion remains constant. In a second one—*dielectric*—obtained in larger electric fields, T_z had decreased enough so that $T_z < T_{el}$. The charges are static and the vertical distortion oscillates around zero (like in our Z model). Figure 15 gives the electrohydrodynamic threshold as a function of the amplitude and frequency of an applied electric field. The experimental data for both square and sine wave excitations are from Galerne[26] and the corresponding theoretical curves from Dubois-Violette.[24] (In practice, the theoretical curve for the square wave agrees with the calculation of Galerne used here.) We see strong resemblances between these curves and our ac results. Their low-frequency results are in the conducting regime. Here the application of a voltage plays two roles. It couples q and n_z (just like the shear s in our problem). It also reduces the relaxation time T_z. For high enough voltage where T_z is small enough, the dielectric regime, which involves oscillations of n_z, is obtained.

An extension of our work including an exact calculation of the instabilty threshold as well as more systematic experiments in particular in the square wave regime is under way. This should give us a better quantitative grasp of the hydrodynamics of nematics.

ACKNOWLEDGMENTS

We acknowledge again the essential contribution due to discussion with and use of the thesis of Y. Galerne. We have had interesting discussions on the subject with E. Dubois-Violette, O. Parodi, and G. Durand. One of us (E.G.) thanks Dr. M. Jericho and his colleagues for a stimulating stay in Canada where part of his work was assembled. Last but not least, the discussions with P. G. de Gennes at crucial points of the experiments have shed a considerable light on the physical mechanisms involved.

APPENDIX A

For an incompressible nematic, the ELP hydrodynamic equations (for the director $\vec{n}$ and the velocity $\vec{v}$) can be written in a linearized form as follows:

Force equation

$$\rho \frac{dv_\beta}{dt} = \partial_\alpha \sigma_{\alpha\beta} , \tag{A1}$$

where the stress tensor (describing pressure effects and viscous dissipation) is

$$\overleftrightarrow{\sigma} = -p\overleftrightarrow{I} + \alpha_4 \overleftrightarrow{A} + \alpha_1(\vec{n}\cdot\overleftrightarrow{A}\cdot\vec{n})\vec{n}\vec{n} + \alpha_2\vec{n}\vec{N} + \alpha_3\vec{N}\vec{n} + \alpha_5\vec{n}(\vec{n}\cdot\overleftrightarrow{A}) + \alpha_6(\vec{n}\cdot\overleftrightarrow{A})\vec{n} , \tag{A2}$$

$$\vec{N} = \frac{d\vec{n}}{dt} - \vec{\omega}\times\vec{n}, \quad \vec{\omega} = \tfrac{1}{2}\vec{\nabla}\times\vec{v},$$

$$A_{\alpha\beta} = \tfrac{1}{2}(\partial_\alpha v_\beta + \partial_\beta v_\alpha) .$$

Applying this equation to the Miesowicz experiment[7] ($d\vec{n}/dt = 0$) leads to

$$\eta_a = \tfrac{1}{2}\alpha_4 ,$$

$$\eta_b = \tfrac{1}{2}(\alpha_3 + \alpha_4 + \alpha_6) , \tag{A4}$$

$$\eta_c = \tfrac{1}{2}(\alpha_4 + \alpha_5 - \alpha_2) . \tag{A5}$$

Torque equation

$$I\frac{d\vec{\Omega}}{dt} = \vec{\Gamma}_{\text{elast}} + \vec{\Gamma}_{\text{visq}} + \vec{\Gamma}_{\text{magn}} + \vec{\Gamma}_{\text{electr}}, \qquad \vec{\Omega} = \vec{n}\times\frac{d\vec{n}}{dt} . \tag{A6}$$

For all practical frequencies, the inertial term to the left can be taken to be zero.

Elastic torque

$$\vec{\Gamma}_{\text{elast}} = \vec{n}\times\vec{h} ,$$

where the molecular field $\vec{h}$

$$\vec{h} = \vec{h}_{\text{splay}} + \vec{h}_{\text{twist}} + \vec{h}_{\text{bend}} \tag{A7}$$

has to be evaluated in term of the Frank elastic constants K_1, K_2, K_3.[13]

Viscous torque

$$\Gamma_{\text{visq}} = -\vec{n}\times[\gamma_1\vec{N} + \gamma_2\overleftrightarrow{A}\cdot\vec{n}] \tag{A8}$$

with

$$\gamma_1 = \alpha_3 - \alpha_2, \quad \gamma_2 = \alpha_3 + \alpha_2 .$$

The expression of Γ_{visq} can be used directly to evaluate the torques on the molecules in the geometry of Figs. 1(b) and 1(c) given by $-\alpha_3\partial v/\partial z$ and $\alpha_2\partial v/\partial z$ and to calculate the equilbrium angle θ_0 such that $tg^2\theta_0 = \alpha_3/\alpha_2$.

Magnetic torque

$$\Gamma_{\text{mag}} = \chi_a(\vec{n}\times\vec{H})(\vec{n}\cdot\vec{H}); \tag{A9}$$

this expresses that the magnetic energy will be lowest when $\vec{n}$ is along the direction of H.

Electric torque

$$\Gamma_{\text{elec}} = \epsilon_a(\vec{n}\times\vec{E})(\vec{n}\cdot\vec{E}) . \tag{A10}$$

In MBBA, $\epsilon_a < 0$ the molecules tend to align perpendicular to $\vec{E}$.

We have five variables ($\vec{n}$ and $\vec{v}$) and only five equations. ($\vec{h}$ is defined within a constant $\vec{h} \to \vec{h} + \lambda\vec{n}$. This can be expressed by looking for the two components obtained by multiplying Eq. (A7) by $X\vec{n}$.)

APPENDIX B: LESLIE EQUATION FOR THE SHEAR-FLOW PROBLEM OF FIG. 1(a)

We look for the most general form of the coupled equations (A1) and (A6) retaining only first-order terms in the instability variables (we consider only a linear instability). We also assume that, as observed experimentally, all derivatives along oy are null:

$$\vec{n} = (1, n_y, n_z)$$

$$2\overleftrightarrow{A} = \begin{vmatrix} 2v_{x,x} & v_{y,x} & (v_{x,z} + v_{z,x}) \\ v_{y,x} & 0 & s \\ v_{x,z} + v_{z,x} & s & 2v_{z,z} \end{vmatrix},$$

$$2\vec{\omega} = \begin{vmatrix} -s \\ v_{x,z} - v_{z,x} \\ v_{y,x} \end{vmatrix},$$

$$\left(v_{a,b} = \frac{\partial v_a}{\partial b}\right).$$

After calculation, we obtain the components of the force $F_\beta = \sigma_{\alpha\beta,\alpha}$,

$$F_x = \alpha_3 \frac{\partial \dot{n}_z}{\partial z} + \eta_B \frac{\partial^2 v_x}{\partial z^2} + \frac{\alpha_3 + \alpha_6}{2} \frac{\partial}{\partial z}(s n_y) + (\alpha_1 + \alpha_4 + \alpha_5 + \alpha_6 - \eta_D) \frac{\partial^2 v_x}{\partial x^2}, \tag{B1}$$

$$F_y = \alpha_2 \frac{\partial \dot{n}_y}{\partial x} + \eta_c \frac{\partial^2 v_y}{\partial x^2} + \frac{\alpha_5 - \alpha_2}{2} \frac{\partial}{\partial x}(s n_z) + \eta_a \frac{\partial s}{\partial z}, \tag{B2}$$

$$F_z = \alpha_2 \frac{\partial \dot{n}_z}{\partial x} + \eta_c \frac{\partial^2 v_z}{\partial x^2} + \frac{\alpha_5 + \alpha_2}{2} \frac{\partial}{\partial x}(s n_y) + (\alpha_4 - \eta_D) \frac{\partial^2 v_z}{\partial z^2}, \tag{B3}$$

with

$$\eta_D = \tfrac{1}{2}(\alpha_2 + \alpha_4 + \alpha_5).$$

The effect of a magnetic field is given by

$$\vec{n} \times \chi_a \vec{H}(\vec{n} \cdot \vec{h}) = |0, \chi_a H^2 n_z, -\chi_a H^2 n_y|. \tag{B4}$$

The effect of the viscous torque can be calculated by expressing

$$\vec{n} \times (\gamma_1 \vec{N} + \gamma_2 \overleftrightarrow{A} \cdot \vec{n}).$$

One finds

$$\begin{vmatrix} 0 \\ \gamma_2 n_z v_{x,x} - \alpha_3(s n_y + v_{x,z}) - \alpha_2 v_{z,x} - \gamma_2 \dot{n}_z \\ -\gamma_2 n_y v_{x,x} + \alpha_2(s n_z + v_{y,x}) + \gamma_1 \dot{n}_y \end{vmatrix}. \tag{B5}$$

The values of the first derivatives of the velocity in (B5) can be incorporated in the director term. We express the x and z dependence of the velocity components as $e^{ik_x x} e^{ik_z z}$ in the force equation $\vec{F} = 0$. For example,

$$\frac{\partial v_x}{\partial z}\left(\eta_1 k_x^2 + \eta_B k_z^2\right) = -\alpha_3 k_z^2 \eta_z - \frac{\alpha_6 + \alpha_3}{2} k_z^2 s n_y$$

or

$$v_{x,z} = \beta_1 \eta_z + \beta_2 s n_y$$

with

$$\beta_1 = -\frac{\alpha_3 k_z^2}{\eta_1 k_x^2 + \eta_B k_z^2},$$

$$\beta_2 = -\frac{(\alpha_6 + \alpha_3) k_z^2}{2(\eta_1 k_x^2 + \eta_B k_z^2)}$$

and similarly

$$v_{z,x} = \beta_3 \eta_z + \beta_y s n_y,$$

$$v_{y,x} = \beta_5 \eta_y + \beta_6 s n_z,$$

$$\beta_3 = -\frac{\alpha_2 k_x^2}{\eta_2 k_z^2 + \eta_c k_x^2},$$

$$\beta_4 = -\frac{(\alpha_2 + \alpha_5) k_x^2}{2(\eta_2 k_z^2 + \eta_c k_x^2)},$$

$$\beta_5 = -\frac{\alpha_2 k_x^2}{\eta_c k_x^2 + \eta_a k_z^2},$$

$$\beta_6 = -\frac{(\alpha_5 - \alpha_2) k_x^2}{2(\eta_c k_x^2 + \eta_a k_z^2)}.$$

Finally, the balance between torques is written

$$\gamma_z \dot{n}_z + (Kk^2 + \chi_a H^2) n_z + (\alpha_3 + \alpha_2\beta_4 + \alpha_3\beta_2) s n_y = 0, \tag{B6}$$

$$\gamma_y \dot{n}_y + (Kk^2 + \chi_a H^2) n_y + (\alpha_2 + \alpha_2\beta_6) s n_z = 0, \tag{B7}$$

with

$$k^2 = k_x^2 + k_z^2,$$

$$\gamma_z = \gamma_1 + \alpha_2\beta_3 + \alpha_3\beta_1 \sim 0.5\gamma_1,$$

$$\gamma_y = \gamma_1 + \alpha_2\beta_5 \sim 0.5\gamma_1$$

for MBBA.[8]

We have assumed a one constant elastic model with $K_1 = K_2 = K_3 = K$. A complete form is quite complex and involves derivatives of n along x and z.

*Supported in part by the Délégation Generale à la Recherche Scientifique et Technique.

[1]A. Saupe, Angew. Chem. (Int. Ed. Engl.) 7, 97 (1968); I. G. Chistyakov, Sov. Phys. Usp. 9, 551 (1967); P. G. de Gennes, *Liquid Crystals Physics* (Oxford U.P., London, to be published).

[2]F. M. Ericksen, Arch. Ration. Mech. Anal. 4, 231 (1960).

[3]F. M. Leslie, Quart. J. Mech. Appl. Math. 19, 357 (1966).

[4]O. Parodi, J. Phys. (Paris) 31, 581 (1970).

[5]Another approach leading to essentially the same picture has been described by the Harvard group. D. Foster, T. C. Lubensky, P. C. Martin, J. Swift, and P. S. Pershan, Phys. Rev. Lett. 26, 1016 (1971).

[6]P. Pieranski, P. Cladis, and C. Williams, Phys. Rev. Lett. 29, 90 (1972).

[7]M. Miesowicz, Nature 158, 27 (1946).

[8]C. H. Gähwiller, Phys. Lett. A 36, 311 (1971).

[9]F. M. Leslie, Arch. Ration. Mech. Anal. 28, 265 (1968).

[10]J. Wähl and F. Fischer, Opt. Commun. 5, 341 (1972).

[11]S. Meiboom and R. C. Hewitt, Phys. Rev. Lett. 30, 261 (1972).

[12]P. Pieranski and E. Guyon, Solid State Commun. 13, 435 (1973).

[13]F. C. Frank, Discuss. Faraday Soc. 25, 1 (1958).

[14]See, for example, H. Zocher, Trans. Faraday Soc. 29, 945 (1933); P. Pieranski, F. Brochard, and E. Guyon, J. Phys. (Paris) 33, 681 (1972).

[15]J. L. Janning, Appl. Phys. Lett. 4, 173 (1972).

[16]E. Guyon, P. Pieranski, M. Boix, Lett. Appl. Eng. Sci. 1, 19 (1972).

[17]N. H. Hartshorne and A. Stuart, *Crystals and the Polarising Microscope* (Edward Arnold Ltd., London, 1970).

[18]J. Williams, J. Chem. Phys. 39, 384 (1963).

[19]W. Helfrich, J. Chem. Phys. 51, 2755 (1969).

[20]P. Pieranski, E. Dubois-Violette, and E. Guyon, Mol. Cryst. Liq. Cryst. (to be published).

[21]A. Rapini (private communication).

[22]For a general discussion of "back flow," see F. Brochard, Mol. Cryst. Liq. Cryst. (to be published).

[23]E. Dubois-Violette, P. G. de Gennes, and O. Parodi, J. Phys. (Paris) 32, 305 (1971).

[24]E. Dubois-Violette, J. Phys. (Paris) 33, 95 (1972).

[25]P. A. Penz and G. W. Ford, Phys. Rev. A 6, 414 (1972).

[26]Y. Galerne, Thèse de 3ème cycle (Orsay, Paris, 1973) (unpublished).

[27]We will see that in a square-wave model there are no instabilities possible when $T_y/T_z=1$. This is a general result in problems of instabilities described by coupled equations as (5.6) and (5.7). Qualitatively, we can say that the component of the instability with the smallest time constant develops first and induces the development of the second component. This fast component would relax to zero but the other slow component will keep the instability present. The mechanism clearly does not work when the two time constants are equal.

[28]F. Brochard, P. Pieranski, and E. Guyon, Phys. Rev. Lett. 28, 1681 (1972).

[29]S. Chandrasekhar, *Hydrodynamic and Hydromagnetic Stability* (Clarendon, London, 1961).

[30]E. Guyon and P. Pieranski, Physica (to be published).